July 2024, Volume 18, Number 3

Iranian Journal of Toxicology
ARAK UNIVERSITY OF MEDICAL SCIENCES

Research Paper

Anti-Colon Cancer Activity of Nano-synthetic Quinolone: *In vivo* and *In vitro* Study

Asmaa Mohamed Attya[1], Mahmoud Ashry[1*], Doaa Galal El-Sahra[2], 4Mohamed A. A. Abdel-Aal[3], Abdelbaset M.A. Abdelreheem[1]

[1] *Zoology Dept., Faculty of Science, Al-Azhar University, Assuit, Egypt*
[2] *Modern University for Technology and Information, Cairo, Egypt*
[3] *Dept. of Pharmaceutical Chemistry, Faculty of Pharmacy, Al-Azhar University, Assuit, Egypt*

Scan to access website

How to cite this paper:
Mohamed Attya A, Ashry M, Galal El-Sahra D, Abdel-Aal M, Abdelreheem A. Anti-Colon Cancer Activity of Nano-synthetic Quinolone: *In vivo* and *In vitro* Study**.** **Iranian Journal of Toxicology.** 2024; 18(3):166-181. doi: 10.32592/IJT.18.3.166

doi: 10.32592/IJT.18.3.166

Article info
Received: 16/02/2024
Accepted: 17/07/2024
Published: 20/07/2024

*** Corresponding author:**
Mahmoud Ashry, Faculty of Science, Al-Azhar University, Assiut, Egypt.
E- mail: mahmoud_ashry20@yahoo.com

ABSTRACT

Background: Colon cancer is one of the most prevalent malignancies in both men and women. This study investigated the anticancer efficacy of a new synthetic form of quinolone nanoparticles (QNPs) against colon cancer cells. As an experimental model, we investigated methods to prevent the development of colon cancer in adult male albino rats induced by 1,2-dimethylhydrazine (DMH).

Methods: Forty adult male rats (weighing 150-200 g) were randomly assigned to four groups of ten as follows: Group 1: Normal rats considered the reference group. Group 2: Normal rats treated intraperitoneally with 100 µg/kg/day of quinolone. Group 3: Rats with induced colon cancer by DMH. Group 4: Rats with colon cancer, as the experimental model, and administered QNPs at 100 µg/kg/day for 6 weeks.

Results: The results showed that QNPs significantly improved the treatment of induced colon cancer in rats. This finding was supported by significant increases in CD4, colon SOD, and GPx activity, as well as in GSH and CAT levels. Further discoveries included a significant decline in the serum values of CEA, CA19-9, AFP, TNF-α, IL1β, ALT, AST, urea, creatinine, cholesterol, triglycerides, colon DNA damage, MDA, and NO. The histopathological results demonstrated the therapeutic potential of QNPs, which were successful in halting the development of colon cancer in an experimental animal model.

Conclusion: The findings of the current study demonstrated that QNPs were able to prevent colon cancer in rats by enhancing their immune system, lowering inflammatory markers, and improving damaged oxidative stress tolerance.

Keywords: Anticancer, Colon cancer, Dimethylhydrazine (DMH), Nanoparticles, Quinolone

Introduction

Colorectal cancer (CRC) ranks as the second most prevalent and lethal cancer worldwide, representing 10% of all cancer cases and 9.4% of all cancer-related deaths globally in 2020 [1]. The onset and progression of CRC are shaped by various risk factors, including lifestyle choices, age, family history, and the intake of red or processed meat as opposed to white meat [2]. Early diagnosis of cancer can save lives; however, CRC is often diagnosed at a stage when symptoms are severe [3]. The process of colorectal carcinogenesis is a multi-step phenomenon driven by genetic alterations in oncogenes and tumor suppressor genes, which lead to the transformation of healthy colonic epithelium into metastatic carcinoma [4]. Moreover, chronic oxidative stress frequently results in DNA damage, mutations in cancer-associated genes, and a detrimental cycle involving cell death, mutations, and an overproduction of reactive oxygen species (ROS) and reactive nitrogen species. These negative effects can all contribute to the progression of CRC.

Currently, various treatments are adopted for (CRC), including chemotherapy, immunotherapy, surgery, radiation, and nutritional supplementation. However, the low success rate of individual CRC therapies continues to be an issue due to the side effects associated with these treatments. Tumor cells rapidly develop resistance to anticancer drugs due to their genetic instability; thus, it is essential to develop new drugs that employ different mechanisms and offer improved therapeutic efficacy [5, 2]. Regarding this, the introduction and development of novel anticancer medications are imperative. These steps necessitate a significant interest and challenges to undertake such studies.

The heterocyclic molecule quinolone, with a chemical formula of C_9H_7N, is based on nitrogen and has a molecular weight of 129.16. Salts can be formed by their reaction with acids, and they exhibit both nucleophilic and electrophilic substitutions [7]. Quinoline and its derivatives are acknowledged heterocyclic compounds

that exhibit a diverse array of pharmacological activities, which encompass antimalarial, anticancer, antiplasmodial, antifungal, and antibacterial effects. Previously, quinoline was chemically modified to create a vast array of different quinoline derivatives, which were then used to create a variety of promising prospects against different forms of cancer and other disorders [7, 8].

Quinolones are a significant class of medication that is now utilized in clinical settings to treat bacteria [9, 10]. They function by inhibiting topoisomerase IV (type 2 topoisomerases) and bacterial gyrase. Certain quinolone medications demonstrate anticancer potential by following their counterparts in mammalian enzymes [11]. Among these compounds, ciprofloxacin has shown promising activity in inducing apoptosis, especially in tumor cells. This has led to a suggestion that it could be utilized as an adjuvant therapy to treat specific malignancies. It has been suggested that altering the quinolone scaffold at position 7 significantly affects its activity and may cause it to be more selective for mammalian enzymes with enhanced anticancer effects [12]. Ciprofloxacin is a drug functionalized at the piperazinyl-N4 with the physiologically significant 4-phenylthiazole-2-acetamide. See Figure 1.

Based on the aforementioned properties of quinolines, medicinal chemists have dedicated their efforts to creating a variety of techniques, which include using organometallic reagents, LiCl, BF3, CuCN, and THF, among others, as well as new computer simulation tools to synthesize various kinds of bioactive quinoline derivatives [13]. Using the DNA-methyl green assay, Katarzyna et al. generated indolo[2,3-b]quinoline derivatives containing a guanidine group, which demonstrated a pronounced selective anticancer effect by serving as a potent inducer of cell apoptosis [14, 15]. The development of drug research in the current, high-tech era of computer processes, such as molecular docking and quantitative structure-activity connection, makes drug synthesis considerably cost-effective and time-efficient [16]. The purpose of this study was to determine whether the synthesized quinolone nanoparticles (QNPs) might exhibit protective properties against 1,2-dimethylhydrazine (DMH)-induced CRC in male rats and their synergistic effect on CRC cell lines.

Materials and Methods

Chemicals: All of the chemicals used in this study, including DMH, were obtained from Sigma Aldrich (St. Louis, Missouri, USA). DMH acts as an initiator of tumors.

Chemistry: H-NMR spectra were recorded at 500 or 400 MHz on JEOL JNM ECX 500 and 400 MHz (JEOL Ltd, Musashino, Akishima, Tokyo, Japan) at the Graduate School of Natural Sciences and Technology, Kanazawa University, Japan or Bruker AVANCE III 400 MHz spectrophotometer (Bruker BioSpin AG, Fällandin, Switzerland) at the Faculty of Science, Sohag University, Sohag, Egypt. C-NMR spectra were recorded at 125 MHz on JEOL JNM ECX 500 MHz (JEOL Ltd, Musashino, Akishima, Tokyo, Japan) at the Graduate School of Natural Sciences and Technology, Kanazawa University, Japan. TMS was used as an internal standard and CDCl3 as a solvent. Chemical shift) δ (values are expressed in parts per million (ppm) and coupling constants) J (in Hertz (Hz). The signals are designated as follows: s, singlet; d, doublet; t, triplet; q, quartet; m, multiplet; brs, broad singlet. Mass spectroscopy and elemental analysis were carried out at the regional center for mycology and biotechnology, Al-Azhar University, Cairo, Egypt. 4-Methylphenacyl bromide 2 was synthesized according to an established procedure [17]. For additional details, please see Appendix 1.

Synthesis of 2-amino-4-p-tolylthiazole 3: The appropriate 4-methylphenacylbromide 2 (0.005 mol) and N-phenylthiourea (0.006 mol) were heated at reflux in ethanol (20 mL) for 2 h. The reaction mixture was cooled, added to water (100 mL), and rendered alkaline with an aqueous solution of sodium acetate. The formed precipitate was collected, dried, and crystallized from ethanol/water [18, 19]. Compound 3 was confirmed by its reported melting points [20].

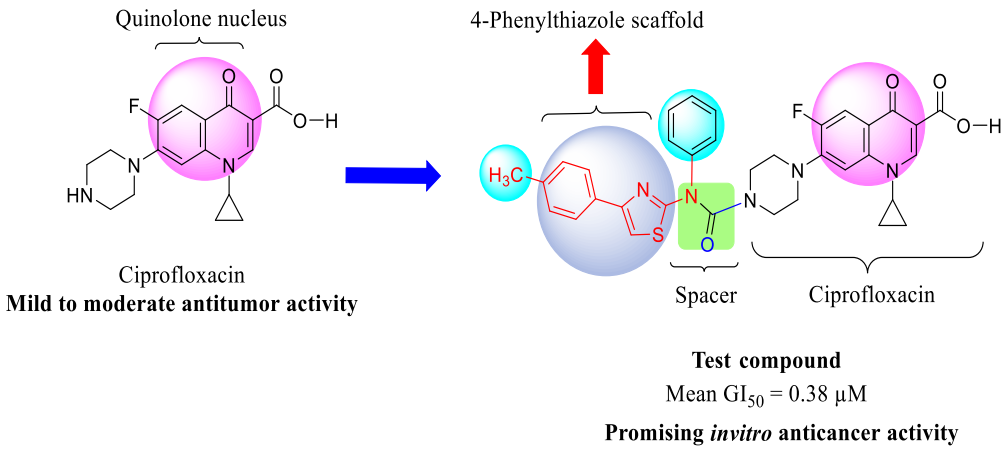

Figure 1: Design of the target compound.

Synthesis of 4-nitrophenyl (4-p-tolylthiazol-2-yl) carbamate 4: A mixture of the 2-amino-4-p-tolylthiazole 3 (0.002 mol), potassium carbonate (0.415 g, 0.006mol) and 4-nitrophenylchloroformate (0.726 g, 0.0026 mol) in dry xylene (10 mL) was heated at reflux for 4-hr. The reaction mixture was cooled to room temperature, shaken vigorously with water (10 mL) then with hexane (10 mL). The formed precipitate in organic phase was filtered off, washed with hexane, dried and crystallized from ethanol. Yield = 0.768 g (89%); beige powder, mp: 9294 ℃ ;1H-NMR (400 MHz, CDCl3 (δ 8.29) d ,J = 9.2 Hz, 2H, ArH), 7.597.49 (m, 7H, ArH), 7.36 (d ,J = 9.2 Hz, 2H, Ar-H), 7.24 (s, 1H, thiazole C5H), 7.14 (d ,J = 7.6 Hz, 2H, ArH), 2.35 (s, 3H, PhCH3 ;(Anal. calculated for C23H17N3O4S: C, 64.03; H, 3.97; N, 9.74; found: C, 64.29; H, 3.81; N, 9.98.

Synthesis of 1-Cyclopropyl-6-fluoro-4-oxo-7-{4-[phenyl (4-(p-tolyl)thiazol-2-yl)carbamoyl]piperazin -1-yl}-1,4-dihydroquinoline-3-carboxylic acid 5i: A mixture of the carbamate intermediate 4 (0.001 mol) and ciprofloxacin (0.331 g, 0.001 mol) in xylene (10 mL) was heated at reflux for 6 h. The formed precipitate was filtered off while hot, washed with xylene then acetonitrile and dried to afford the pure product [22]. Yield 0.418 g (67%); off white powder, mp: 26870 ℃ ;1H-NMR (500 MHz, CDCl3 (δ 8.69 (s, 1H, C2H), 7.94 (d ,J = 12.7 Hz, 1H, C5H), 7.68 (d ,J = 6.9 Hz, 2H, ArH), 7.497.44 (m, 4H, C8H & 3ArH), 7.397.30 (m, 2H, ArH), 7.15 (d ,J = 6.9 Hz, 2H, ArH), 7.08 (s, 1H, thiazole C5H), 3.753.60 (m, 4H, piperazinyl-H), 3.473.35 (m, 1H, cyclopropyl-H), 3.313.14 (m, 4H, piperazinyl-H), 2.33 (s, 3H, PhCH3 ,(1.321.22) m, 2H, cyclopropyl-H), 1.171.06 (m, 2H, cyclopropyl-H;(13C-NMR (125 MHz, CDCl3 (δ 177.14 ,166.98 , 164.32 ,157.24 ,153.98) d ,JCF = 249.5 Hz), 151.07, 147.59, 142.13, 139.01, 137.93, 131.72, 129.64, 129.41, 127.66, 127.13, 125.96, 120.40, 116.67, 112.59 (d ,JCF = 25.8 Hz), 108.23, 107.66, 105.24, 49.42, 45.52, 35.34, 21.36, 8.22; MS m/z calculated for C34H30FN5O4S [M :[+623.20 ,found:623.99; Anal. calculated for C34H30FN5O4S: C, 65.47; H, 4.85; N, 11.23; found: C, 65.26; H, 4.60; N, 11.39. [21]. For additional details, please see Appendix 3.

Biological Assays

Anticancer Screening: Briefly, screening is a two-stage process, beginning with the evaluation of all compounds against the 60 cell lines at a single dose of 10-5 molar (10 uM). Compounds which exhibit significant growth inhibition are again evaluated against the 60 cell lines panel at five concentration levels, 10-fold dilutions each with the top dose being 10-4 molar (100 uM). Experimental drugs solubilized in dimethyl sulfoxide (DMSO) at designated concentrations are added to cell lines and incubated for 48-hr at 37ºC. End point determinations were made with a protein binding dye, SRB, and evaluated spectro-photometrically. Results for each tested compound were reported as percent of growth of treated cells compared to untreated controls. Using the seven absorbance measurements, both control and test growth in the presence of drug at the five concentrations (Ti). The percent growth was calculated at each of the drug concentrations [22]. For additional details, please see Appendix 4.

Molecular Mechanism Study of Anticancer Activity of the Target Compounds: Different steps of molecular mechanism study were carried out at the Division of Chemical Biology and Medicinal Chemistry, College of Pharmacy, University of Texas at Austin, USA. The molecular docking was performed at the Pharmaceutical Chemistry Department, Faculty of Pharmacy, Al-Azhar University, Assiut Branch, Egypt.

Expression, Purification, and Activation of Protein Kinases: Human, recombinant full-length CDK1/ CyclinA2 Kinase or human and recombinant full-length CDK2/CyclinA2 Kinase were co-expressed by baculovirus in Sf9 insect cells using an *N*-terminal GST tag on both proteins (Promega). Activated full-length ERK2 (Rattus norvegicus mitogen-activated protein kinase 1, GenBank accession number NM_053842) was purified from bacteria and activated following the previously described protocol [23]. Human JNK2α2 (GenBank accession number NM_002752) was expressed, purified, and activated as described previously [24, 25]. The p38MAPKα was expressed, purified, and activated as described previously [22]. The activated kinases were prepared in storage buffer [25mM HEPES (pH 7.5), 2 mM DTT, 50 mM KCl, 0.1 mM EDTA, 0.1 mM EGTA, and 10-20% (v/v) glycerol] and were stored at -80ºC.

Expression and purification of different kinase substrates: GST-ATF2 (1-115), His-Ets-1 (1-138), and GST-c-Jun (1-221) were expressed and purified according to previously established protocols [26]. Native histone H1 was purified from calf thymus tissues (Promega).

Kinase Activity Assay:

For CDK1/Cycline A2 and CDK2/Cycline A2 assays ,1 ng CDK1 or 1.6 ng CDK2 was assayed with 200 ng native Histone H1 protein substrate in 25 µL reaction volume .For ERK2 assays ,4 nM ERK was assayed with 10 µM Ets1 (1-138) protein substrate .

For JNK assays, 25 nM active JNK2α2 were assayed with 2 µM GST-c-Jun) 1221 .(

For p38MAPKα assays, 10 nM active enzyme was assayed with 10 µM GST-ATF2) Δ 1-115) protein substrate .

In all assays, the reaction was started by the addition of radio labeled 50 µM (For CDK1/2 assays) or 500 µM [γ-32P] ATP (100-1000 c.p.m. pmol-1 (for all other kinases.

Kinase activity was quantified at different inhibitor concentrations by determination of the initial rates of the reaction. At each time point (0.5, 1, 1.5, 2, 4 min) 10 µL aliquots were withdrawn from every reaction and spotted to 2×2 cm2 squares of P81 cellulose paper; the papers were washed for 3×15 minutes in 50 mM phosphoric acid (H3PO4 (then the c.p.m associated with

each paper were quantified in Perkin Elmer Tri-Carb Liquid Scintillation Counter. In order to estimate the IC50 of each tested inhibitor, dose-response curves for data confirming to inhibition were fitted to the equation:

Parameters: The parameters used for deriving equation 1 are defined as follows ;

i, concentration of inhibitor I, observed rate; , is the observed rate in the absence of inhibitor, is the observed rate constant at saturating inhibitor, I, is the concentration that leads to half the maximal change in. [27]. For additional details, please see Appendix 5.

Cell Culture: The A549 cell line was cultured in RPMI (Invitrogen) supplemented with 1X Glutamax (Invitrogen), 10% (v/v) US-grade Fetal Bovine Serum (Invitrogen), 100 µg/mL streptomycin (Sigma), and 100 U/mL penicillin (Sigma). The cells were cultured in a humidified incubator with 5% CO_2 at 37°C. For Western blot analyses, cells were seeded at a density of 800,000 to 1,000,000 cells per well in a 6-well plate and allowed to incubate for 24 h. Following this, they were treated with DMSO or different concentrations of each inhibitor for another 24 h.

Western Blots: The primary antibodies were incubated overnight at 4ºC using 1:1000 anti-Rb (4H1) Mouse mAb (Cell Signaling Technology); 1:1000 anti-phospho-Rb (Ser807/811) (D20B12) XP ®Rabbit mAb (Cell Signaling Technology); 1:1000 anti-PP1α Antibody (Cell Signaling Technology);1:1000 anti-phospho-PP1α (Thr320) Antibody (Cell Signaling Technology); 1:2000 anti-phospho-p44/42 MAPK (ERK1/2) (Thr202/Tyr204) (E10) mouse mAb (Cell Signaling Technology); 1:1000 antiphospho-H2AX (Ser-139), rabbit mAb (Cell Signaling Technology); 1:1000 anti-H2AX (D17A3) rabbit mAb (Cell Signaling Technology); 1:1000 anti-PARP (46D11) rabbit mAB (Cell Signaling Technology); 1:1000 anti-cleaved-PARP (D214) rabbit polyclonal Abs (Cell Signaling Technology); 1/2000 anti-Vinculin (E1E9V) XP rabbit mAb (Cell Signaling Technology) and 1:5000 anti-actin, clone 4 mouse mAb (Millipore). Either anti-rabbit (Bio-Rad) or anti-mouse (Cell Signaling Technology) horseradish peroxidase-conjugated secondary antibodies and Western Bright ECL Western Blotting Reagents (Advansta) were used to develop the blots. All experiments were reproduced in independent experiments. All experiments were performed in duplicate. For additional details, please see Appendix 6.

Cell Proliferation Assays: Cell proliferation was assessed by utilizing the CellTiter 96® AQueous One Solution Reagent (Promega). A total of 2000 cells were plated in each well of a 96-well plate. The cells were exposed to different concentrations of each inhibitor in a final volume of 100 µL of media. After 48 h, 20 µL of the reagent was added to each well, which was then incubated for another 2 h before measuring the absorbance at 490 nm.

IncuCyte Single Cell Apoptosis Analysis: The number of 2000 A549 cells were seeded in each well of a 96-well plate. After 24 h, cells were treated with varying concentrations of 5h and 5r in full media, which included a fixed concentration of the lncuCyte Caspase-3/7 reagent according to the manufacturer's protocol. The cells were then incubated and imaged using lncuCyte® ZOOM equipment with a ×10 objective at specified time intervals. The cells were then incubated and imaged using lncuCyte® ZOOM equipment with a ×10 objective at specified time intervals. Once the cells reached confluence, the count of apoptotic cells was adjusted to reflect the percentage in order to account for cell proliferation.

Experimental Design: Male adult Wistar albino rats (n=40) weighing 150-200 g were used in this study. They were acquired from the Animal Colony at the National Research Center in Cairo, Egypt. For one week, the animals were kept in appropriate plastic cages to get adjusted to the environment. Standard rodent pellet foods and extra tap water were always accessible to them. Every animal was given human care in accordance with the normative guidelines established by the Faculty of Science at Al-Azhar University in Assuit, Egypt, regarding the care and utilization of experimental animals (approval code: AZHAR 19/2022).

Induction of Colon Cancer: Colon cancer was induced in the rats through the administration of DMH (Sigma Aldrich, St. Louis, USA) [28]. The DMH was dissolved in a solution of 1 mM sodium bicarbonate combined with 1 mM ethylene diamine tetra-acetic acid at a pH of 6.5. Over a duration of 15 weeks, the animals were given weekly intraperitoneal injections of DMH in the groin at a dosage of 30 mg/kg body weight.

Animal Grouping: Following CRC induction, four groups of rats (n=10 each) were randomly reorganized to include both cancer and normal rats. The normal animals in the first group were given 2 mL of distilled water (pH 6.8) orally as a control. Quinolone NPs (100 µg/kg) were administered daily to the second group of normal rats. The third group consisted of animals with CRC induced by DMH; however, they received no treatment and served as a positive control. Lastly, the fourth group, consisting of rats with induced CRC, received QNP intraperitoneally as a potential anticancer treatment for 6 weeks.

Blood and Tissue Sampling: Upon completion of the treatment period, the rats were weighed and subjected to an overnight fasting period. Following the induction of anesthesia with diethyl ether, blood samples were collected from the retro-orbital plexus utilizing sterile, heparinized glass capillaries. The entire blood samples were then centrifuged at 3000 rpm for 10 min, allowing for the separation of serum, which was aliquoted and subsequently stored at -80°C until needed for further biochemical analyses. After the collection of blood samples, the rats were sacrificed, and their colonic tissues were carefully dissected. Each colon was bisected, with one portion immersed in a 10% formalin-saline buffer for histological processing and

microscopic examination. The other portion was dried, wrapped in aluminum foil, and stored at -80°C for further biochemical analyses.

Tissue Homogenization: Tissue homogenates (10% w/v) were prepared by homogenizing colon samples in ice-cold phosphate buffer (50 mM, pH 7.4). The nuclear and mitochondrial fractions were extracted from the homogenate by centrifuging them at 5000 rpm for 20 min. The supernatants were then separated into aliquots and kept at -80°C until later biochemical measurements.

Biochemical Determinations: Spectrophotometric analyses were conducted to determine the levels of serum urea, alanine aminotransferase (ALAT), aspartate aminotransferase (ASAT), creatinine, triglycerides, cholesterol, low-density lipoprotein (LDL), and high-density lipoprotein (HDL) cholesterol. These measurements were performed using reagent kits obtained from Biodiagnostic (Dokki, Giza, Egypt).

Oxidative and Antioxidant Determinations: The enzyme-linked immunosorbent assay (ELISA) kits for rat reagents from Sunlong Biotech Co. in Hangzhou, China, were utilized to assess the levels of colon glutathione (GSH), malondialdehyde (MDA), and nitric oxide (NO), as well as the activities of catalase (CAT), superoxide dismutase (SOD), and glutathione peroxidase (GPx) using the Dynatech Microplate Reader Model MR 5000.

Colon DNA Fragmentation Percentage: After cleaving the DNA from intact chromatin, the sample was subjected to centrifugation, followed by the measurement of DNA content in both the supernatant and the pellet. Subsequently, the diphenylamine assay was utilized to evaluate DNA damage, and the extent of DNA fragmentation in the colon was quantified as a percentage [29]. Based on absorbance readings at 578 nm, the percentage of fragmented DNA was calculated using the following formula: the ratio of DNA in the supernatant to the total amount of DNA in the pellet and supernatant characterizes the degree of DNA fragmentation.

Biomarker and Immune-cytokines: Rat reagent ELISA kits from SinoGeneClon Biotech Co., Hang Zhou, China, were employed to assess the concentrations of carcinoembryonic antigen (CEA), carbohydrate antigen 19-9 (CA19-9), tumor necrosis alpha (TNF-α), alpha-fetoprotein (AFP) levels, interlukin-1 beta (IL-1β), and CD4 using the ELISA technique (Dynatech Microplate Reader Model MR 5000).

Histopathology: All animal colon specimens were dissected as soon as possible after death; paraffin sections with a thickness of 5 µm were subsequently analyzed using a light microscope and stained with hematoxylin and eosin [30].

Statistical Analyses: The collected data were analyzed using the Statistical Analysis System (SAS, Institute Inc., Cary, NC, USA, copyright (c) 1998) software. An ANOVA was performed, followed by the Duncan multiple post hoc test, with a significance threshold set at $P \leq 0.05$, according to the methodology outlined by Steel and Torrie [31].

Results

Chemistry: The test compound was synthesized following the method outlined in Figure 2. 4-Methyl acetophenone 1 was reacted with NBS in the presence of *p*-TSA to produce 4-methylphenacylbromide 2. The subsequent reaction of intermediate 2 with *N*-phenylthiourea led to the formation of *N*-phenyl-4-(p-tolyl) thiazol-2-amine 3. This compound was then treated with 4-nitrophenyl chloroformate in the presence of potassium carbonate to yield the corresponding carbamate intermediate 4. Finally, intermediate 3 was reacted with ciprofloxacin to attain the target compound 5. The chemical structure of the synthesized compound was confirmed by using H-NMR, C-NMR, mass spectroscopy, and elemental analyses.

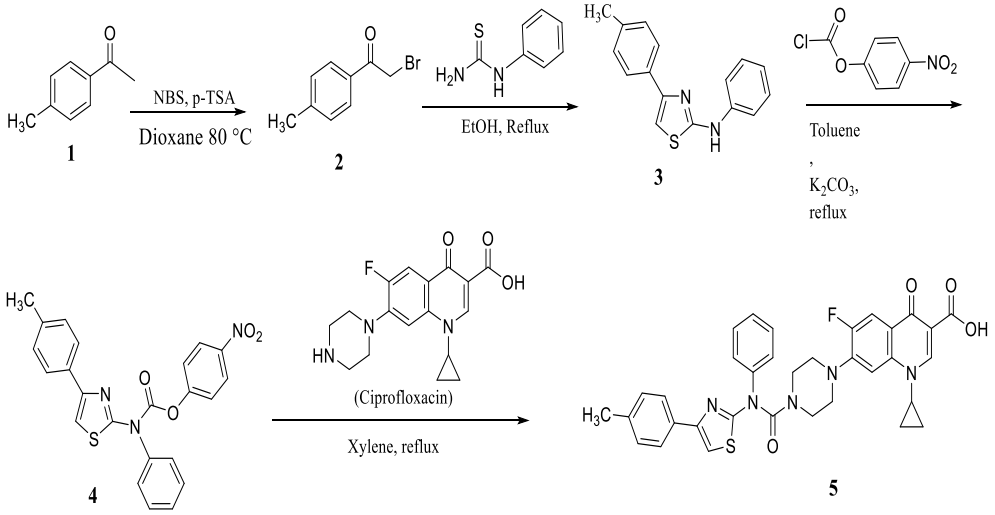

Figure 2: Synthesis of the target compound NP3.

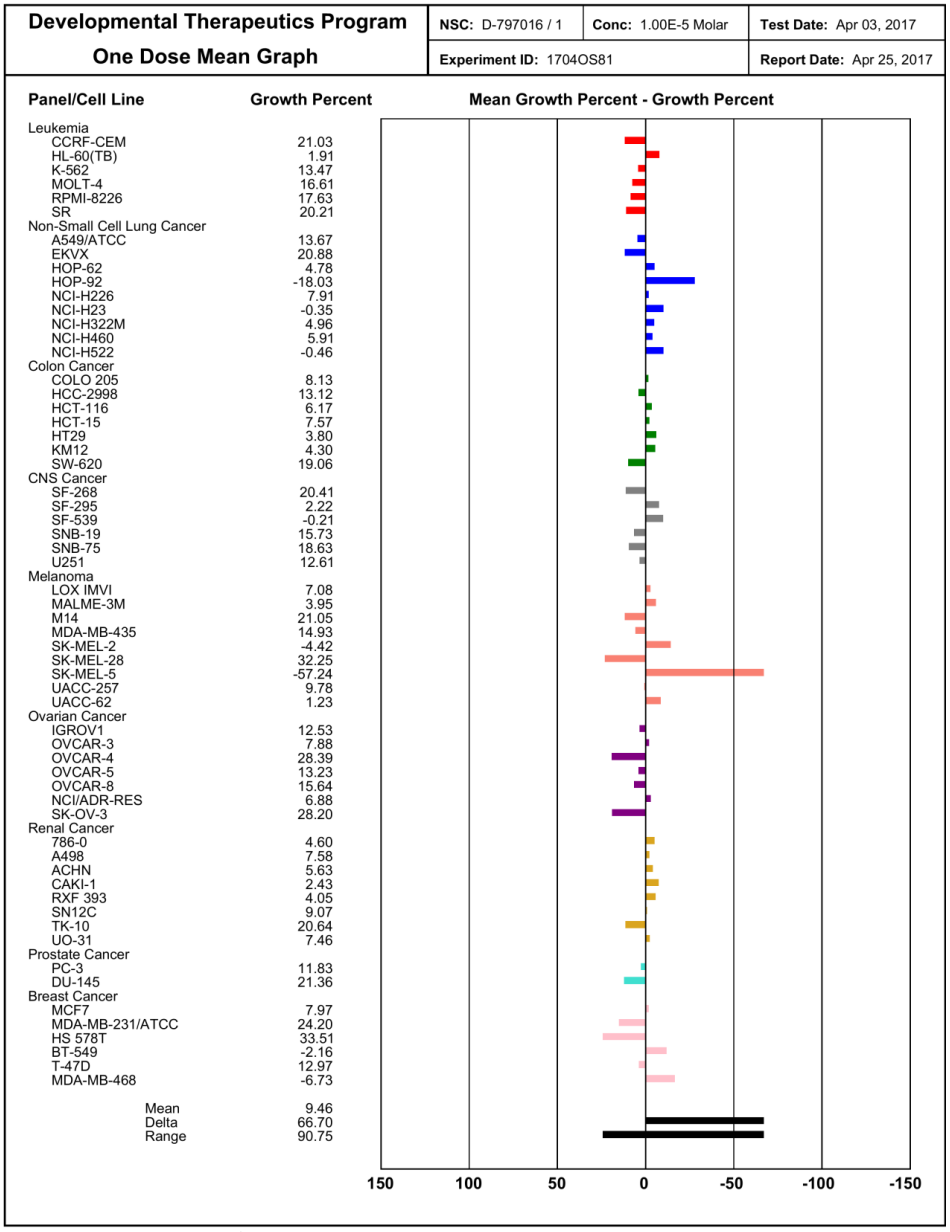

Figure 3: One-dose growth (%) and mean graph of the test compound.

Biological Investigations

Screening of Anticancer Activity: The test compound was selected by the NCI, Bethesda, USA, for *in vitro* anticancer screening in accordance with their drug evaluation protocol. It underwent screening against a panel of 60 cell lines (NCI-60 cell line panel) derived from 9 different types of cancers, including melanoma, leukemia, lung, ovarian, colon, prostate, renal, breast, and central nervous system (CNS). The test compound was initially administered at a concentration of 10 µM, with a culture incubation period of 48 h. Cellular growth was terminated using a protein-binding dye, sulforhodamine B (SRB). The screening results for each compound were documented as the growth percentage of tumor cells treated with the test compound relative to that of the untreated control cells. The negative values represent the occurrence of cancer cell death and a decline in the initial cell count.

***In Vitro* 1-dose Assay:** The test compound revealed potent and broad-spectrum antiproliferative activity. It resulted in complete cell death against Non-Small Cell Lung Cancer HOP-92, HOP-92, NCI-H522, CNS Cancer (SF-539), Melanoma SK-MEL-2, SK-MEL-5, breast cancer BT-549, and MDA-MB-468 (-18.03%, -18.03%, -0.46%, -0.21%, -4.42%, -57.24%, -2.16%, and -6.73%), in addition to a remarkable activity toward the remaining tumor cells (Figure 3). ***In Vitro* 5-dose Assay:** Given the significant growth inhibition observed in the initial screening at 10 µM, the test compounds were chosen for advanced five-dose testing against a panel of 60 tumor cell lines. The compound was screened at five different concentrations: 0.01, 0.1, 1, 10, and 100 µM. Screening results were used to construct dose-response curves (log concentration versus growth percentage), as well as three response parameters were calculated for each cell line: growth inhibition 50% (GI_{50}), total growth inhibition (TGI), and

lethal concentration 50% (LC_{50}).

The GI_{50} value, indicative of growth inhibitory activity, represents the concentration of the compound that inhibits net cell growth by 50%. The TGI value, reflective of cytostatic activity, denotes the concentration that achieves total growth inhibition. Lastly, the LC_{50} value, indicative of cytotoxic activity, signifies the concentration that results in a 50% loss of the initial cell population.

The test compound revealed a significant antitumor activity with GI_{50} values at sub-micromolar concentrations, 0.25 to 0.55 µM, against all examined cell lines. The compound also achieved a total cell growth inhibition with some of the investigated cell lines at a concentration range of 0.89 to 36.10 µM (Table 1).

Table 1: Screening results of compound **5i** at five-dose levels in µM.

Panel	Cell line	GI_{50} (Conc. per cell line)	TGI (Conc. Per cell line)	LC_{50}
Leukemia	CCRF-CEM	-	> 100	> 100
	HL-60(TB)	-	4.76	> 100
	K-562	0.27	> 100	> 100
	MOLT-4	-	-	> 100
	RPMI-8226	0.37	-	> 100
	SR	0.25	> 100	> 100
Non-small cell lung cancer	A549/ATCC	0.37	> 100	> 100
	EKVX	0.41	> 100	> 100
	HOP-62	0.55	96.1	> 100
	HOP-92	0.25	7.63	> 100
	NCI-H226	0.28	87.7	> 100
	NCI-H23	0.32	39.5	> 100
	NCI-H322M	0.32	> 100	> 100
	NCI-H460	0.33	> 100	> 100
	NCI-H522	0.30	9.14	> 100
Colon cancer	COLO 205	-	> 100	> 100
	HCC-2998	0.54	> 100	> 100
	HCT-116	0.32	> 100	> 100
	HCT-15	-	> 100	> 100
	HT29	-	> 100	> 100
	KM12	0.37	> 100	> 100
	SW-620	-	> 100	> 100
CNS cancer	SF-268	0.43	> 100	> 100
	SF-295	0.30	23.7	> 100
	SF-539	0.33	> 100	> 100
	SNB-19	0.43	> 100	> 100
	SNB-75	0.44	20.5	> 100
	U251	0.40	16.1	90.8
Melanoma	LOX IMVI	0.31	> 100	> 100
	MALME-3M	0.37	5.83	> 100
	M14	0.39	> 100	> 100
	MDA-MB-435	-	> 100	> 100
	SK-MEL-2	0.40	6.85	> 100
	SK-MEL-28	-	> 100	> 100
	SK-MEL-5	0.54	3.92	8.73
	UACC-257	-	8.24	> 100
	UACC-62	0.31	37.9	> 100
Ovarian Cancer	IGROV1	0.39	> 100	> 100
	OVCAR-3	0.39	34.6	> 100
	OVCAR-4	-	> 100	> 100
	OVCAR-5	-	> 100	> 100
	OVCAR-8	0.40	50.9	> 100
	NCI/ADR-RES	-	> 100	> 100
	SK-OV-3	0.47	8.13	> 100
Renal Cancer	786-0	0.29	22.5	> 100
	ACHN	0.28	22.1	> 100
	CAKI-1	0.37	> 100	> 100
	RXF 393	0.38	54.6	> 100
	SN12C	-	> 100	> 100
	TK-10	0.53	27.9	> 100
	UO-31	-	> 100	> 100
Prostate Cancer	PC-3	-	> 100	> 100
	DU-145	0.46	33.7	> 100
Breast Cancer	MCF7	-	> 100	> 100
	MDA-MB-231/ATCC	0.38	> 100	> 100
	HS 578T	0.45	> 100	> 100
	BT-549	0.32	> 100	> 100
	T-47D	-	66.1	> 100
	MDA-MB-468	0.37	25.5	> 100
Mean GI_{50}		0.38		

- = Not determined

***In Vitro* Repeated 5-dose Assay:** According to the protocol of the NCI for evaluating anticancer compounds, candidates with promising activity at five-dose screening are further selected for "repeated five-dose assay" to be screened again at five concentration levels toward tumor cells of the NCI cell line panel. Screening results of the test compound showed an outstanding broa-spectrum antitumor activity against all the tested cell lines, with GI_{50} values ranging between 0.04 and 0.58 µM. Furthermore, a total cellar arrest was observed in a number of cancer cells, with TGI values ranging from 0.44 to 22.0 µM (Table 2).

Evaluation of CDK1/CDK2 Inhibitory Activity: The assay is particularly effective for evaluating the impact

Table 2: Screening results of compound **5i** at five-dose levels in µM.

Panel	Cell line	GI_{50} (Conc. per cell line)	TGI (Conc. Per cell line)	LC_{50}
Leukemia	CCRF-CEM	-	> 100	> 100
	HL-60(TB)	-	-	> 100
	K-562	-	> 100	> 100
	MOLT-4	-	> 100	> 100
	RPMI-8226	-	> 100	> 100
	SR	0.22	> 100	> 100
Non-small cell lung cancer	A549/ATCC	-	> 100	> 100
	EKVX	0.36	> 100	> 100
	HOP-62	0.28	21.4	> 100
	HOP-92	0.19	0.72	> 100
	NCI-H226	0.34	> 100	> 100
	NCI-H23	0.29	> 100	> 100
	NCI-H322M	0.24	-	> 100
	NCI-H460	ND[a]	-	> 100
	NCI-H522	-	> 100	> 100
Colon cancer	COLO 205	0.38	-	> 100
	HCC-2998	-	> 100	> 100
	HCT-116	0.35	> 100	> 100
	HCT-15	-	> 100	> 100
	HT29	-	> 100	> 100
	KM12	-	> 100	> 100
	SW-620	-	> 100	> 100
CNS cancer	SF-268	-	> 100	> 100
	SF-295	0.27	-	> 100
	SF-539	0.27	-	> 100
	SNB-19	0.34	> 100	> 100
	SNB-75	0.29	1.54	51.10
	U251	0.34	16.9	> 100
Melanoma	LOX IMVI	-	> 100	> 100
	MALME-3M	0.24	-	> 100
	M14	-	> 100	> 100
	MDA-MB-435	-	-	> 100
	SK-MEL-2	0.30	12.6	> 100
	SK-MEL-28	0.58	> 100	> 100
	SK-MEL-5	-	-	ND[c]
	UACC-257	0.37	> 100	> 100
	UACC-62	-	-	> 100
Ovarian Cancer	IGROV1	0.29	> 100	> 100
	OVCAR-3	-	> 100	> 100
	OVCAR-4	-	> 100	> 100
	OVCAR-5	-	> 100	> 100
	OVCAR-8	0.42	> 100	> 100
	NCI/ADR-RES	-	> 100	> 100
	SK-OV-3	0.25	0.79	> 100
Renal Cancer	786-0	0.30	2.47	> 100
	A498	0.04	0.44	> 100
	ACHN	0.20	-	> 100
	CAKI-1	-	> 100	> 100
	RXF 393	0.35	22.00	> 100
	SN12C	-	> 100	> 100
	TK-10	0.55	12.10	> 100
	UO-31	-	-	> 100
Prostate Cancer	PC-3	-	-	> 100
	DU-145	-	> 100	> 100
Breast Cancer	MCF7	-	> 100	> 100
	MDA-MB-231/ATCC	0.31	-	> 100
	HS 578T	0.41	> 100	> 100
	BT-549	0.28	-	> 100
	T-47D	0.38	> 100	> 100
	MDA-MB-468	0.28	-	> 100
Mean GI_{50}		0.31		

- = Not determined.

of chemical compounds on the activity of a wide array of purified kinases, rendering it suitable for both primary screening and kinase selectivity profiling. The ADP-Glo™ Kinase Assay is capable of monitoring the activity of nearly any enzyme that generates ADP, including ATPases and kinases, utilizing ATP concentrations of up to 1 mM. The test compound experienced a potent inhibitory activity toward both CDK1 and CDK2 (IC_{50}=2.1 and 1.0 µM, respectively). This result correlates to the anticancer activity, proposing these enzymes as possible molecular targets for the activity of compounds.

Effects on CDK Substrates Phosphorylation in Cancer Cells: The test compound was examined for its potential to inhibit CDK substrate phosphorylation in non-small cell lung cancer cell line A549 [33] by treating the cells with different concentrations of the compound. Rb, a proximal substrate for G1 CDK complexes, has its phosphorylation regulated by CDK2 activity, and its phosphorylation state signifies its function as a tumor suppressor in cancer cells. As a potent CDK2 inhibitor *in vitro* (IC_{50}=1.0 µM), the compound under investigation revealed a potential to inhibit Rb phosphorylation at a concentration range of 1-10 µM (Figure 4).

PP1α phosphatase represents a well-known substrate of CDK1 complexes. CDK1 was reported to phosphorylate PP1α on Thr320, and inhibiting the activity of CDK1 kinases results in the suppression of the phosphorylation at this site. The test compound could suppress the phosphorylation PP1α at concentrations 10-25, owing to its potent activity toward CDK1 (*in vitro* IC_{50}=2.1 µM).

Apoptosis Induction as the 2nd Mechanism of Cell Death: Cell cycle arrest in the G1/S phase can be tolerated by most cancer cells, while the arrest in the G2 phase most likely leads to cell death. In order to investigate the mechanism of antitumor activity, the test compound was added at different doses to A549 cells for 24 h. Western blotting was applied to indicate the inhibitor effect on the DNA damage marker (γH2AX) and the apoptosis marker (cleaved PARP). In addition to the induction of DNA damage, apoptosis represents an important process for cell death. Treatment of A549 cells with different concentrations of the test compound resulted in the elevation of apoptosis induction marker (i.e., cleaved PARP level) (Figure 5).

Synergistic Effect of QNPs on Colon Tumor Invasion: In comparison to the control group, the *in vivo* data revealed a significant reduction in CD4 levels alongside significant rises in TNF-α, AFP, CA19-9, CEA, and IL-1β in the CRC group induced by DMH. It is noteworthy that, in comparison to the colon tumor-modeled group, treatment of DMH-induced colon tumor rats with the produced QNPs significantly improved serum levels of CEA, CA19-9, TNF-α, AFP, IL-1β, and CD4 (Table 3).

The administration of prepared QNPs to healthy rats never interferes with liver or kidney function; however, the injection of DMH led to a significant elevation of kidney and liver function markers, as indicated by the significantly increased serum liver enzymes (ASAT and ALAT) and the elevated serum kidney markers (creatinine and urea) when compared to normal rats. Quinolone NP treatment significantly reduced the DMH-induced hepatic and renal impairments in colon cancer-modeled rats (Table 4).

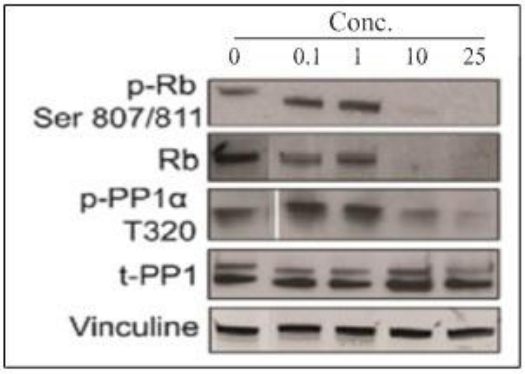

Figure 4: Inhibitory activity of the test compound toward kinases in A549 cancer cell line.

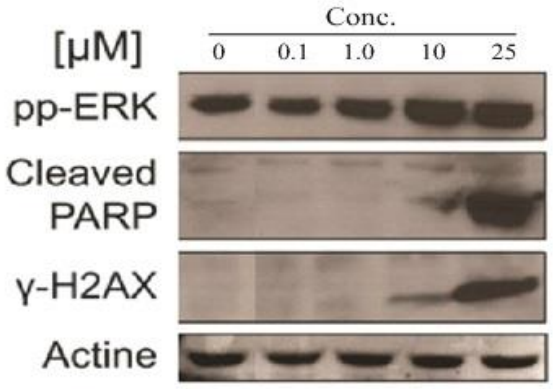

Figure 5: Induction of DNA damage and apoptosis in A549 cell line by the test compound (whole-cell extracts of A549 cells treated with different doses of test compounds for 24 hours).

Table 3: Serum CA19.9, CEA, TNF-α, CD4 and IL-1β levels of normal, colon cancer and colon cancer-treated rats

Groups	CA19.9 (U/mL)	CEA (U/mL)	TNF-α (ng/L)	IL-1β (ng/L)	CD4+ (U/mL)
Control	23.7±3.7	11.5±2.4	126.7±23.9	28.2±8.59	35.4±4.8
NPs (Q)	22.9±5.6	10.5±1.1	117.2±13.8	26.9±7.10	34.1±7.0
DMH	153.7±33.9*	36.9±2.8*	364.67±56.9*	114.3±18.7*	15.6±12.1*
DMH~NPs (Q)	82.1±27.0#	19.6±3.3#	189.9±51.3#	63.6±23.9#	29.8±14.9#

Data are presented as mean ±standard error; data were subjected to one-way ANOVA followed by post hoc (Tukey) test at $p \leq 0.05$. Symbol (*) is significantly different from control group; symbol (#) is significantly different from DMH group at $p \leq 0.05$ level. DMH: Dimethyl Hydrazine; NPs (Q): Nano-form synthetic (Quinolone).

Table 4: Serum liver and kidney functions of normal, colon cancer and colon cancer-treated rats.

Groups	ALAT (U/L)	ASAT (U/L)	Creatinine (mg/dl)	Urea (mg/dl)
Control	47.9±2.03	53.02±5.6	1.1±.0.15	51.5±6.6
NPs (Q)	40.1±3.09	45.01±8.6	0.92±0.13	41.9±5.6
DMH	110.17±6.8*	129.6±13.9*	1.9±0.09*	77.9±7.8*
DMH~NPs (Q)	65.663±7.6#	89.6±10.4#	1.2±0.08#	43.2±4.7#

Data are presented as mean ±standard error; data were subjected to one-way ANOVA followed by post hoc (Tukey) test at p≤ 0.05. Symbol (*) is significantly different from control group; symbol (#) is significantly different from DMH group at $p \leq 0.05$ level. DMH: Dimethyl Hydrazine; NPs (Q): Nano-form synthetic (Quinolone).

Quinolone NPs administration to the healthy control group did not worsen the serum lipid profile; however, DMH intoxication resulted in the onset of atherosclerosis due to a significant decrease in HDL cholesterol and a significant boost in serum total cholesterol, triglycerides, and LDL cholesterol. However, when comparing the group of colon cancer-modeled animals with the rats treated with post-treatment QNPs, there was a significant improvement in all lipid profile measures (Table 5).

Rats injected with DMH also showed significantly altered oxidative status and DNA damage in their colon tissue; this was demonstrated by a significant increase in oxidative power (MDA and NO) and a significant decrease in antioxidant battery (GSH, SOD, CAT, GPx, and DNA fragmentation) when compared to the normal control group. Colon cancer-model rats that were subsequently treated with QNPs exhibited a significant increase in SOD and DNA fragmentation activity, a decrease in levels of colon NO and MDA, and decompensation of the depleted colon GSH, as compared to the corresponding measurements in the untreated cancer-model group (Figure 6).

Table 5: Serum lipid profile of normal, colon cancer and colon cancer-treated rats.

	CHO (mg/dl)	TRG (mg/dl)	HDL (mg/dl)	LDL (mg/dl)
Control	187.9±9.6	185.4±6.10	42.2±3.6	108.6±13.6
NPs (Q)	186.1±16.2	178.0±24.9	40.3±3.30	117.1±6.9
DMH	258.5±40.4*	242.1±43.8*	36.6±1.9*	168.2±45.6*
DMH~NPs (Q)	160.6±11.1#	124.8±10.1#	41.8±1.1#	92.4±10.4#

Data are presented as mean ±standard error; data were subjected to one-way ANOVA followed by post hoc (Tukey) test at p≤ 0.05. Symbol (*) is significantly different from control group; symbol (#) is significantly different from DMH group at $p \leq 0.05$ level. DMH: Dimethyl Hydrazine; NPs (Q): Nano-form synthetic (Quinolone).

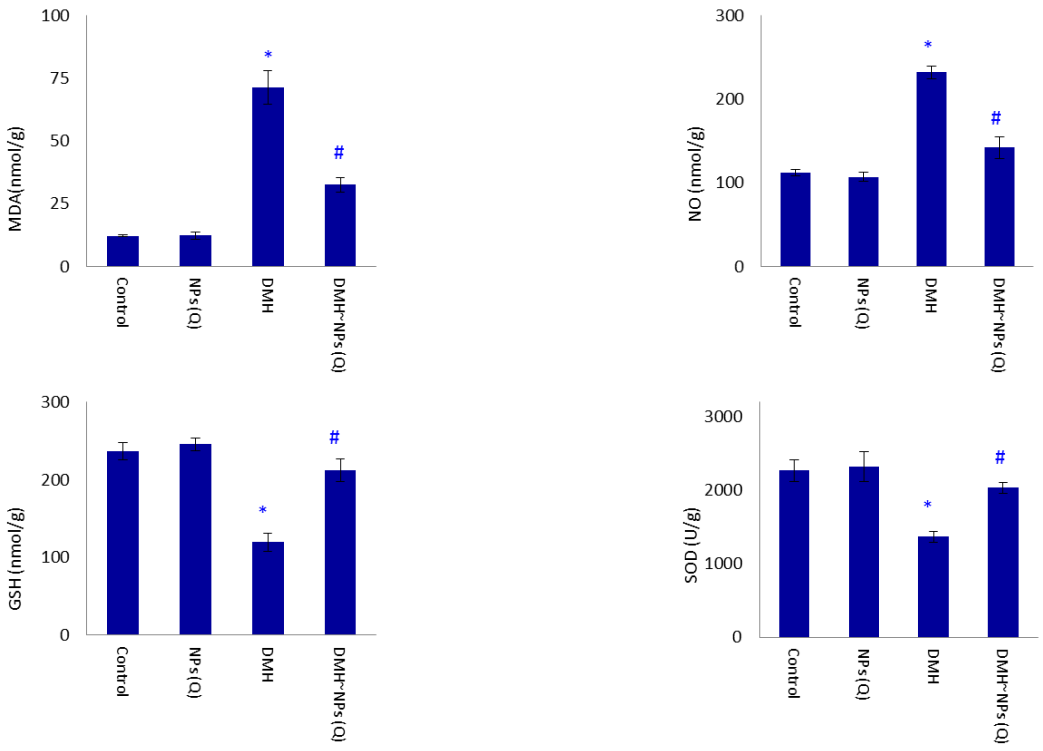

Figure 6: Colon oxidant-antioxidant markers of control, colon cancer and colon cancer-treated rats. Symbol (*) is significantly different from control group; symbol (#) is significantly different from DMH group at $p \leq 0.05$ level. DMH: Dimethyl Hydrazine; NPs (Q): Nano-form synthetic (Quinolone).

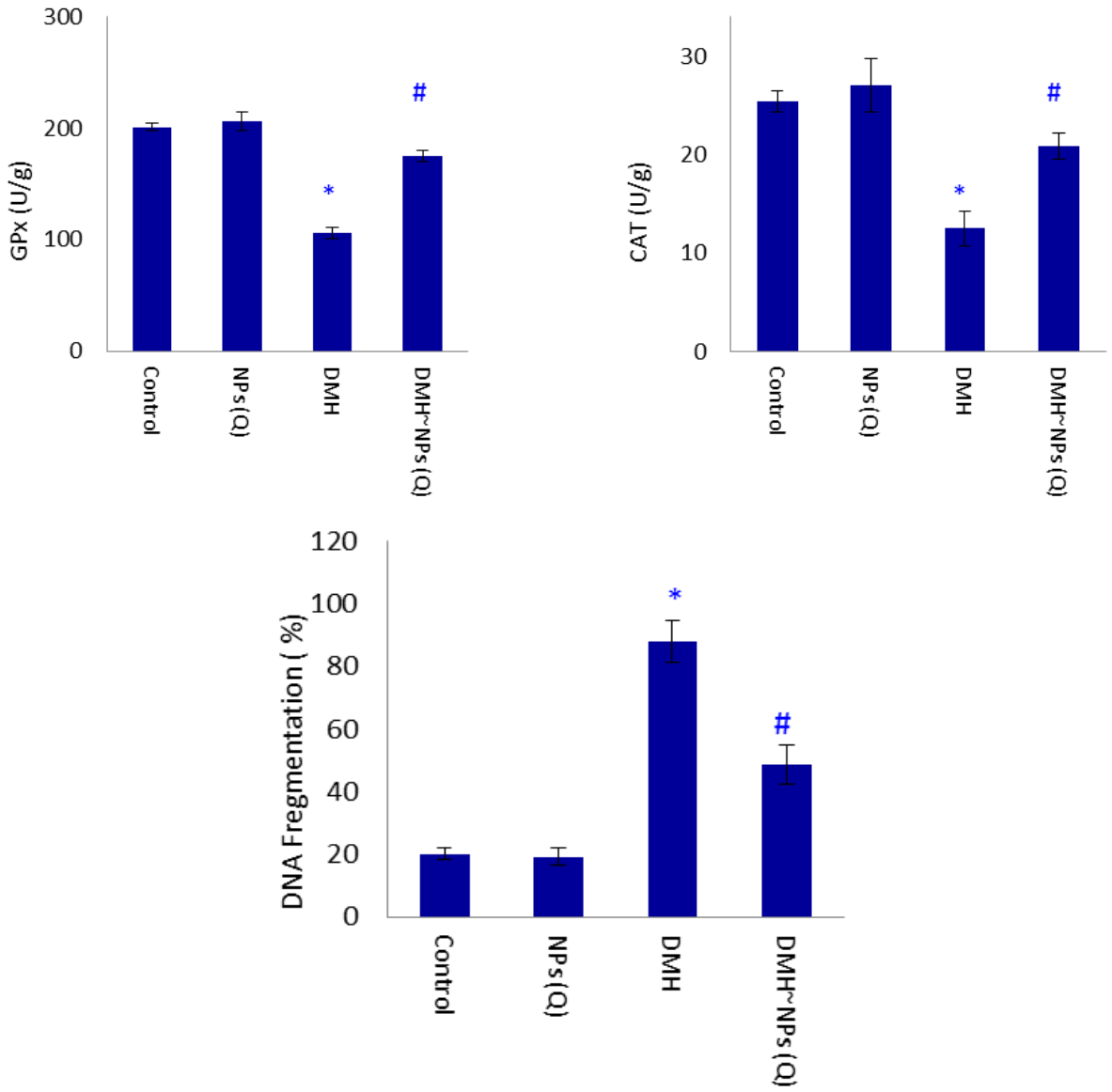

Figure 6 continue: Colon oxidant-antioxidant markers of control, colon cancer and colon cancer-treated rats. Symbol (*) is significantly different from control group; symbol (#) is significantly different from DMH group at $p \leq 0.05$ level. DMH: Dimethyl Hydrazine; NPs (Q): Nano-form synthetic (Quinolone).

Histopathological Examinations: Figure 7 Legend: Photomicrographs presented the histopathological variations of colon tissue sections between inspected groups as follows: Colon Sections of Negative Control Group (A, B & C), synthetic compound QNPs demonstrating intact tissue layers, including tunica mucosa with simple columnar absorptive epithelium (thick arrow), lamina propria homing dense irregular connective tissue (arrowhead) as well as intestinal gland with huge number of goblet cells (wave arrow), tunica sub mucosa comprising loose connective tissue and blood vessels (cube), and smooth muscular layer (circle). (D, E, F) Colon Sections of Cancer (DMH) Group highlighting sloughing and degenerative changes in the epithelial layer (thick arrow) as well as intestinal gland (triangle), and severe aggregation of neoplastic cells along mucosal and submucosal layers (cube). Intestinal gland marked high dysplasia (wave arrow). Aggregated neoplastic cells existed with pleomorphic shapes (arrowhead). Necrotic areas (thin arrow) coupled with edema leading to dispersion between smooth muscle fibers (circle) were also detected. (H, I & J) Colon Sections of Cancer~Synthetic Compound QNPs group: revealing obvious recovery along tissue structure. Pronounced reduction in numbers of neoplastic cells (cube) and surrounded by connective tissue (wave arrow), and intact muscular layer (circle). *Keys* - Stain: Hematoxylin & Eosin. Magnification Power: x100, x200, x400. Scale Bars: 500 µm, 100 µm, 50 µm.

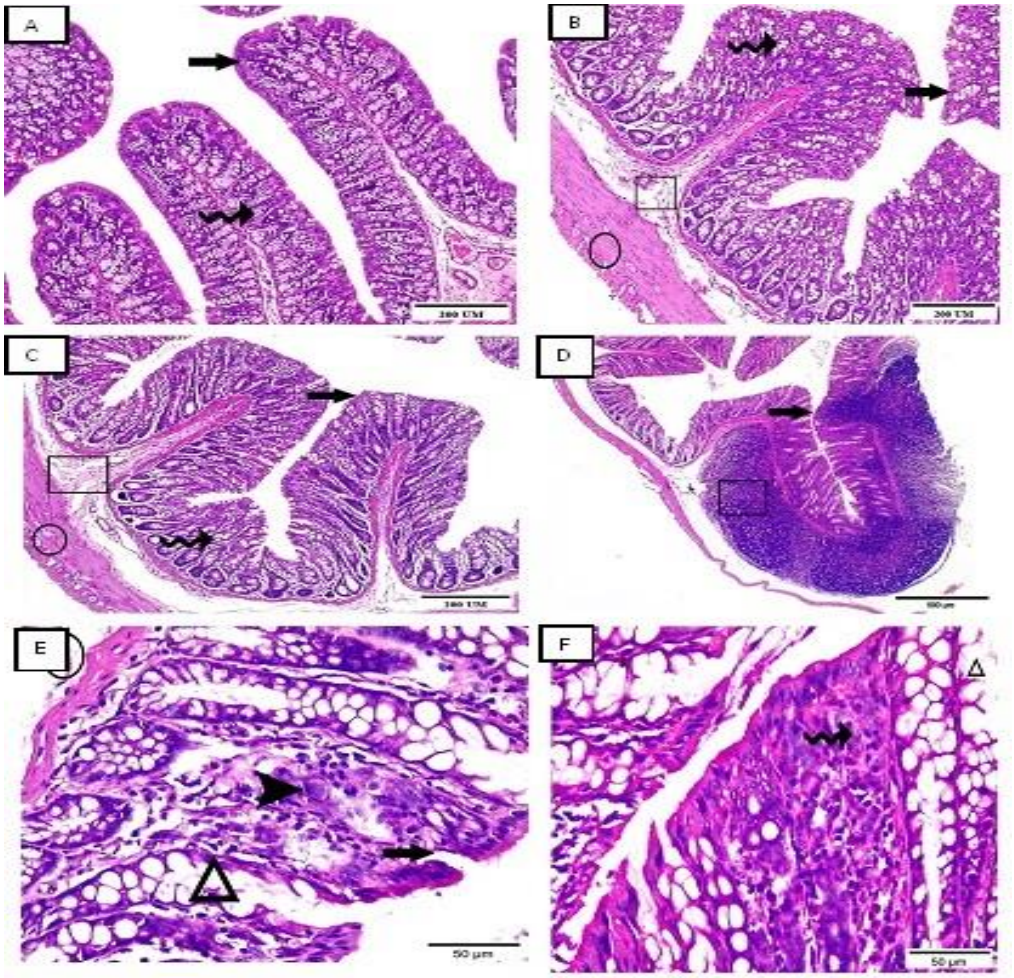

Figure 7: Photomicrographs of various colon tissue sections.
Descriptions: A, B & C: Colon sections of negative control group, synthetic compound QNPs demonstrating intact tissue layers including tunica mucosa with simple columnar absorptive epithelium (thick arrow), lamina propria homing dense irregular connective tissue (arrowhead) as well as intestinal gland with huge number of goblet cells (wave arrow), tunica sub mucosa comprising loose connective tissue and blood vessels (cube), and smooth muscular layer (circle). **D, E & F:** Colon Sections of Cancer (DMH) Group highlighting sloughing and degenerative changes in epithelial layer (thick arrow) as well as intestinal gland (triangle), and severe aggregation of neoplastic cells along mucosal and submucosal layers (cube). Intestinal gland marked high dysplasia (wave arrow). Aggregated neoplastic cells existed with pleomorphic shapes (arrowhead). Necrotic areas (thin arrow) coupled with edema leading to dispersion between smooth muscle fibers (circle) were also detected. (Hematoxylin & Eosin Stain. Magnification: =x100, x200, x400 & Scale Bar= 500µm, 100µm, 50µm).

Discussion

Colon cancer is the second most frequent type of cancer worldwide [1]. Due to early identification and insufficient treatment options, its rates are rapidly increasing. Furthermore, the quality of life of patients is adversely affected by the major side effects of anticancer drugs used to treat CRC. Consequently, the primary disadvantage of an efficient CRC treatment is a reduced vulnerability to chemotherapy and a higher risk of adverse effects [28]. The basis for this investigation was the potential therapeutic and antioxidant qualities of quinolones as a novel anticancer medication with minimal side effects.

It is commonly recognized that quinolénes mainly function via binding to DNA topoisomerases, particularly type II enzymes [32-34]. After testing the newly synthesized molecule against topoisomerase I and II enzymes, it was found to have minor inhibitory action that was inconsistent with its anticancer potential, indicating the possibility of another molecular target or targets for activity. Kinase inhibitors that target several CDKs have the potential to be highly effective anticancer medicines, as demonstrated by multiple well-established reports [35, 36]. Using ADP-Glo™ kinase assay kits, the test compounds were assessed for their capacity to prevent recombinant human full-length CDK1/Cycline A2 and CDK2/Cycline A2 from phosphorylating native Histone H1 *in vitro* [37, 38]. This assay, known as a luminous kinase test, quantifies the amount of ADP generated by a kinase reaction in which ADP is transformed into ATP, which is then transformed into light by ultra-Glo™ Luciferase. The amount of ADP and kinase activity is strongly correlated with the luminosity signal.

Most cancer cells can withstand cell cycle arrest in the G1/S phase; nevertheless, cell death is most likely to result from cell cycle arrest in the G2 phase. For 24 h, A549 cells were treated with various dosages of the test chemical in order to examine the mechanism of

anticancer action. To determine the inhibitory effect on the apoptosis marker (i.e., cleaved PARP) and the DNA damage marker (i.e., γH2AX), western blotting was utilized. A crucial indicator of DNA damage is the phosphorylation of the DNA damage response signaling protein γH2AX at Ser139 [39]. The test chemical was able to consistently induce γH2AX phosphorylation at a concentration of 10 µM in a dose-dependent manner.

Apoptosis is a crucial step in the process of cell death, in addition to the generation of DNA damage. When A549 cells were treated with varying concentrations of the test chemical, the levels of cleaved PARP and the apoptosis induction marker increased [39]. These findings suggest that the anticancer effectiveness of the newly identified CDK inhibitor may be linked to the induction of apoptosis and cell cycle arrest at the G2 phase [36]. It is commonly recognized that cancer cells are unable to withstand cellular arrest during the G2 phase, which almost certainly results in cell death [40].

In rats with CRC, there were elevated levels of pro-inflammatory cytokines (IL-1β and TNF) and tumor markers (CA19-9, CEA, and AFP), alongside a reduction in apoptotic biomarkers (CD4), which aligns with findings from previous studies [4, 28]. The production of ROS plays a crucial role in the imbalance between antioxidants and oxidants. It is a well-established step in the progression of CRC induced by DMH. The primary cause of DMH-induced colon cancer involves its biotransformation into more reactive intermediates, facilitated by cytochrome P450 monooxygenases and GSH conjugation-dependent oxidation during the first and second phases of metabolism [41]. Reactive oxygen species damage the colon and cause instability in colon cell metabolism, leading to positive changes in CEA, CA19-9, and AFP in the bloodstream. This study further indicates that elevated blood concentrations of CA19-9 and CEA are correlated with the presence of colon cancer or significantly larger lesion sizes and higher adenoma counts [42]. Treatment with QNPs reduces the growth of tumors, and several recent reports indicate that QNPs may be used as anticancer medicines. Their underlying mechanism of action demonstrates anticancer properties against a number of cancer subtypes [43].

In this study, rats given a CRC model had significantly higher serum levels of creatinine and urea, as well as ALAT and ASAT activities. This significant rise in activity could be due to the hepatocytes' membrane losing its cellular functional integrity as a result of highly reactive electrophiles that seriously harm the liver by methylating nucleobases, causing necrosis and fatty infiltration, and disrupting the polysomal assembly and enzymes that are present [44]. A sign of renal illness is elevated creatinine levels [45]. Here, QNPs either modify the antioxidant defense system and lower lipid peroxidation or diminish hepato-nephrotoxicity by providing free radicals with an electron to lessen their reactivity [43].

Following DMH injection, elevated serum cholesterol and triglyceride levels were seen, which is in line with findings reported by Abdel-Hamid *et al*. [46]. They claimed that there was a positive correlation between the concentration of serum triglycerides and the synthesis of bile acid, which may encourage the development of large-intestine cancer. Furthermore, a different study found a link between increased levels of triglycerides and total cholesterol and colorectal polyps [47].

A colon-specific carcinogen called DMH is used to cause CRC in rodents. By methylating biomolecules in the colon's epithelial cells, the methyldiazonium ion stimulates oxidative stress. Exposure to carcinogens is the primary cause of most colon cancers. The cells may thereafter undergo a sequence of precancerous lesion, premalignant, and malignant phases as they develop [48]. The lowered activities of antioxidant enzymes enhance the formation of free radicals that surpass the antioxidant system's scavenging capability in cancer [49]. SOD and CAT are more susceptible to oxidative damage generated by the carcinogen treatment. Therefore, other organs may also exhibit enzymatic alterations.

Conclusions

The current study concludes that synthetic QNPs have therapeutic promise in fighting colon cancer. The new synthetic agent caused a significant improvement in immune-inflammatory markers, oxidative state, histological features, and relevant biomarkers. The significant anticancer property of QNPs is likely linked to its ability to activate CD4 cells, which induce cell apoptosis. It is also possible that QNPs could become a potential future medication for the treatment and perhaps even prevention of cancer. Further research is warranted to explore the potential pharmacologic properties of QNPs against cancer.

Conflict of Interests

The authors declare no conflict of interest with any entity.

Funding

This study was funded by the authors and did not receive funds from any external sources.

Acknowledgement

The authors wish to thank the professors and staff of the Zoology and Pharmaceutical Chemistry Depart ments in the Faculties of Pharmacy and Science, Al-Azhar University, Assuit, Egypt, for their valuable support toward this research project.

Compliance with Ethical Guidelines

This study was conducted consistent with the ethical guidelines approved by the Ethics Committee of the Faculty of Science, Al-Azhar University, Assuit (approved number AZHAR, 25/2022)

Authors' Contributions

Conceptualization: Mahmoud Ashry, Abdelbaset M.A. Abdelreheem, and Asmaa Mohammed Attya. Methodology, Investigation, Writing-original draft:

Mohamed A.A Abdel-Aal. Histopathology: All authors. Supervision and Writing-review and editing: Mahmoud Ashry, Asmaa Mohammed Attya, Abdelbaset M.A. Abdelreheem, Doaa Galal El-Sahra, Mohamed A.A Abdel-Aal.

APPENDICES

The following appendices are expanded information from the literature regarding the materials presented in the **Materials and Methods** section.

Appendix 1

Chemistry: H-NMR spectra were recorded at 500 or 400 MHz on JEOL JNM ECX 500 and 400 MHz (JEOL Ltd, Musashino, Akishima, Tokyo, Japan) at the Graduate School of Natural Sciences and Technology, Kanazawa University, Japan, or Bruker AVANCE III 400 MHz spectrophotometer (Bruker BioSpin AG, Fällandin, Switzerland) at the Faculty of Science, Sohag University, Sohag, Egypt. C-NMR spectra were recorded at 125 MHz on JEOL JNM ECX 500 MHz (JEOL Ltd, Musashino, Akishima, Tokyo, Japan) at the Graduate School of Natural Sciences and Technology, Kanazawa University, Japan. TMS was used as an internal standard, and $CDCl_3$ as a solvent. Chemical shift (δ) values are expressed in parts per million (ppm) and coupling constants (J) in Hertz (Hz). The signals are designated as follows: s, singlet; d, doublet; t, triplet; q, quartet; m, multiplet; brs, broad singlet. Mass spectroscopy and elemental analysis were carried out at the Regional Center for Mycology and Biotechnology, Al-Azhar University, Cairo, Egypt. 4-Methylphena cylbromide 2 was synthesized according to an established procedure [18].

Appendix 2

Synthesis of 4-nitrophenyl ….: Yield = 0.768 g (89%); beige powder, mp: 92–94℃; ^{1}H-NMR (400 MHz, $CDCl_3$) δ 8.29 (d, J = 9.2 Hz, 2H, Ar–H), 7.59–7.49 (m, 7H, Ar–H), 7.36 (d, J = 9.2 Hz, 2H, Ar-H), 7.24 (s, 1H, thiazole C5–H), 7.14 (d, J = 7.6 Hz, 2H, Ar–H), 2.35 (s, 3H, Ph–CH_3); Anal. calculated for $C_{23}H_{17}N_3O_4S$: C, 64.03; H, 3.97; N, 9.74; found: C, 64.29; H, 3.81; N, 9.98.

Appendix 3

Synthesis of 1-Cyclopropyl ….: Yield 0.418 g (67%); off white powder, mp: 268–70℃; ^{1}H-NMR (500 MHz, $CDCl_3$) δ 8.69 (s, 1H, C2–H), 7.94 (d, J = 12.7 Hz, 1H, C5–H), 7.68 (d, J = 6.9 Hz, 2H, Ar–H), 7.49–7.44 (m, 4H, C8–H & 3Ar–H), 7.39–7.30 (m, 2H, Ar–H), 7.15 (d, J = 6.9 Hz, 2H, Ar–H), 7.08 (s, 1H, thiazole C5–H), 3.75–3.60 (m, 4H, piperazinyl-H), 3.47–3.35 (m, 1H, cyclopropyl-H), 3.31–3.14 (m, 4H, piperazinyl-H), 2.33 (s, 3H, Ph–CH_3), 1.32–1.22 (m, 2H, cyclopropyl-H), 1.17–1.06 (m, 2H, cyclopropyl-H);^{13}C-NMR (125 MHz, $CDCl_3$) δ 177.14, 166.98, 164.32, 157.24, 153.98 (d, J_{C-F} = 249.5 Hz), 151.07, 147.59, 142.13, 139.01, 137.93, 131.72, 129.64, 129.41, 127.66, 127.13, 125.96, 120.40, 116.67, 112.59 (d, J_{C-F} = 25.8 Hz), 108.23, 107.66, 105.24, 49.42, 45.52, 35.34, 21.36, 8.22; MS m/z calculated for $C_{34}H_{30}FN_5O_4S$ [M^+]: 623.20, found:623.99; Anal. calculated for $C_{34}H_{30}FN_5O_4S$: C, 65.47; H, 4.85; N, 11.23; found: C, 65.26; H, 4.60; N, 11.39.

Appendix 4

Anticancer Screening: Briefly, screening is a two-stage process, beginning with the evaluation of all compounds against the 60 cell lines at a single dose of 10^{-5} molar (10 uM). Compounds that exhibit significant growth inhibition are reevaluated against the 60 cell lines panel at five concentration levels, with 10-fold dilutions each, with the top dose being 10^{-4} molar (100 uM). Experimental drugs solubilized in dimethyl sulfoxide (DMSO) at designated concentrations are added to cell lines and incubated for 48 h at 37ºC. End-point determinations were made with a protein binding dye, SRB, and evaluated spectro-photometrically. Results for each tested compound were reported as the growth percent of treated cells compared to untreated controls. Using the seven absorbance measurements, both control and test growth were assessed in the presence of the drug at the five concentrations (Ti). The percent growth was calculated at each of the drug concentrations.

The percent growth inhibition was calculated as: [(Ti-Tz)/(C-Tz)] x 100 for concentrations for which Ti>/= Tz and [(Ti-Tz)/Tz] x 100 for concentrations for which Ti<Tz. Three dose-response parameters were calculated for each experimental agent. Growth inhibition of 50% (GI_{50}) is calculated from [(Ti-Tz)/(C-Tz)] x 100 = 50, which is the drug concentration resulting in a 50% reduction in the net protein increase (as measured by SRB staining) in control cells during the drug incubation. The drug concentration resulting in total growth inhibition (TGI) is calculated from Ti = Tz. The LC_{50} (concentration of drug resulting in a 50% reduction in the measured protein at the end of the drug treatment as compared to that at the beginning) indicating a net loss of cells following treatment is calculated from [(Ti-Tz)/Tz] x 100 = -50. Values are calculated for each of these three parameters if the level of activity is reached. However, if the effect is not reached or is exceeded, the value for that parameter is expressed as greater or less than the maximum or minimum concentration tested.

Appendix 5

Kinase Activity Assay [28]**:**

- ***For CDK1/Cycline A2* and *CDK2/Cycline A2 assays***, 1 ng CDK1 or 1.6 ng CDK2 was assayed with 200 ng native Histone H1 protein substrate in 25 µL reaction volume.
- ***For ERK2 assays,*** 4 nM ERK was assayed with 10 µM Ets1 (1-138) protein substrate.
- ***For JNK assays***, 25 nM active JNK2α2 were assayed with 2 µM GST-c-Jun (1–221).
- ***For p38MAPKα assays,*** 10 nM active enzyme was assayed with 10 µM GST-ATF2 (Δ 1-115) protein substrate.

- ***In all assays***, the reaction was started by the addition of radiolabeled 50 µM (For CDK1/2 assays) or 500 µM [γ-^{32}P] ATP (100-1000 c.p.m. pmol^{-1}) for all other kinases.
- ***Kinase activity*** was quantified at different inhibitor concentrations by determining the initial rates of the reaction. At each time point (0.5, 1, 1.5, 2, 4 min), 10 µL aliquots were withdrawn from every reaction and spotted to 2×2 cm^2 squares of P81 cellulose paper; the papers were washed for 3×15 min in 50 mM phosphoric acid (H_3PO_4), then the c.p.m associated with each paper were quantified in Perkin Elmer Tri-Carb Liquid Scintillation Counter. In order to estimate the IC_{50} of each tested inhibitor, dose-response curves for data confirming inhibition were fitted to the equation:

$$V_0 = V_{00} - \left(V_{00} \frac{i}{i + (K_{50})} \right) + V'$$

- ***Parameters:*** The parameters used for deriving equation 1 are defined as follows;

i, concentration of inhibitor I; V_0, observed rate; V_{00}, is the observed rate in the absence of inhibitor, V' is the observed rate constant at saturating inhibitor, I, K_{50} is the concentration that leads to half the maximal change in V_0.

Appendix 6

Western Blots: The primary antibodies were incubated overnight at 4ºC using 1:1000 anti-Rb (4H1) Mouse mAb (Cell Signaling Technology); 1:1000 anti-phospho-Rb (Ser807/811) (D20B12) XP® Rabbit mAb (Cell Signaling Technology); 1:1000 anti-PP1α Antibody (Cell Signaling Technology);1:1000 anti-phospho-PP1α (Thr320) Antibody (Cell Signaling Technology); 1:2000 anti-phospho-p44/42 MAPK (ERK1/2) (Thr202/Tyr204) (E10) mouse mAb (Cell Signaling Technology); 1:1000 antiphospho-H2AX (Ser-139), rabbit mAb (Cell Signaling Technology); 1:1000 anti-H2AX (D17A3) rabbit mAb (Cell Signaling Technology); 1:1000 anti-PARP (46D11) rabbit mAB (Cell Signaling Technology); 1:1000 anti-cleaved-PARP (D214) rabbit polyclonal Abs (Cell Signaling Technology); 1/2000 anti-Vinculin (E1E9V) XP rabbit mAb (Cell Signaling Technology) and 1:5000 anti-actin, clone 4 mouse mAb (Millipore). Either anti-rabbit (Bio-Rad) or anti-mouse (Cell Signaling Technology) horseradish peroxidase-conjugated secondary antibodies and Western Bright ECL Western Blotting Reagents (Advansta) were used to develop the blots. All experiments were reproduced in independent experiments. All experiments were performed in duplicate.

References

1. Wang C, Qiao X, Wang J, Yang J, Yang C, Qiao Y, Guan Y, Wen A, Jiang L. Amelioration of DMH-induced colon cancer by eupafolin through the reprogramming of apoptosis-associated p53/Bcl2/Bax signaling in rats. Eur J Inflamm. 2022;**20**:20587392211069771. [**doi**: 10.1177/20587392211069771]
2. El-Khadragy MF, Nabil HM, Hassan BN, Tohamy AA, Waaer HF, Yehia HM, Alharbi AM, Moneim AE. Bone marrow cell therapy on 1, 2-dimethylhydrazine (DMH)-induced colon cancer in rats. Cell Physiol Biochem. 2018;**45**(3):1072-83. [**doi**: 10.1159/000487349] [**Pmid**: 29439258]
3. Nabil HM, Hassan BN, Tohamy AA, Waaer HF, Abdel Moneim AE: Radioprotection of 1, 2-dimethylhydrazine-initiated colon cancer in rats using low-dose gamma rays by modulating multidrug resistance-1, cytokeratin 20, and beta-catenin expression. Hum Exp Toxicol.2016;**35**(3): 282-92. [**doi**: 10.1177/0960327115584687] [**pmid**: 25926526]
4. Alkhuriji AF, Alsaiari SG, Alomar SY, Alnafjan AA, Alobaid H, El-Khadragy MF. Effect of mesenchymal stem cells on cytochrome-c release and inflammation in colon cancer induced by 1,2-dimethylhydrazine in Wistar albino rats. Biosci Rep. 2021;**41**(3):BSR20204356. [**doi**: 10.1042/BSR20204356] [**pmid**: 33604610]
5. Du W, Elemento O. Cancer systems biology: embracing complexity to develop better anticancer therapeutic strategies. Oncogene. 2015;**34** (25):3215-25. [**doi**: 10.1038/onc.2014.291] [**pmid**: 25220419]
6. Marella A, Tanwar OP, Saha R, Ali MR, Srivastava S, Akhter M, Shaquiquzzaman M, Alam MM. Quinoline: A versatile heterocyclic. Saudi Pharm J. 2013;**21**(1):1-12. [**doi**: 10.1016/j.jsps.2012.03.002] [**pmid**: 23960814]
7. Hussaini SM. Therapeutic significance of quinolines: a patent review (2013-2015). Expert Opin Ther Pat. 2016;**26**(10):1201-21. [**doi**: 10.1080/13543776.2016.1216545] [**pmid**: 27458877]
8. Jain S, Chandra V, Jain KP, Pathak K, Pathak D, Vaidya A. Comprehensive review on current developments of quinoline-based anticancer agents. Arab J Chem. 2016:**12**(8):4920-46. [**doi**: 10.1016/j.arabjc.2016.10.009]
9. Naeem A, Badshah SL, Muska M, Ahmad N & Khan K. The current case of quinolones: synthetic approaches and antibacterial activity. Molecules. 2016;**21**(4):268. [**doi**: 10.3390/molecules21040268] [**pmid**: 27043501]
10. Pranger AD, van der Werf TS, Kosterink JGW, Alffenaar JWC. The Role of Fluoroquinolones in the Treatment of Tuberculosis in 2019. Drugs. 2019;**79**(2):161-71. [**doi**: 10.1007/s40265-018-1043-y] [**pmid**: 30617959]
11. Bisacchi GS, Hale MR. A "Double-Edged" Scaffold: Antitumor Power within the Antibacterial Quinolone. Curr Med Chem. 2016;**23**(6):520-77. [**doi**: 10.2174/0929867323666151223095839] [**pmid**: 26695512]
12. Abdel-Aal MAA, Abdel-Aziz SA, Shaykoon MSA, Abuo-Rahma GEA. Towards anticancer fluoroquinolones: A review article. Arch Pharm (Weinheim). 2019;352(7):e1800376. [**doi**: 10.1002/ardp.201800376] [**pmid**: 31215674]
13. Kumar S, Bawa S, Gupta H. Biological activities of quinoline derivatives. Mini Rev Med Chem. 2009;**9**(14):1648-54. [**doi**: 10.2174/138955709791012247] [**pmid**: 20088783]
14. Sidoryk K, Świtalska M, Jaromin A, Cmoch P, Bujak I, Kaczmarska M,et.al.The synthesis of indolo [2, 3-b] quinoline derivatives with a guanidine group: Highly selective cytotoxic agents. Eur J Med Chem. 2015;105:208-19. [**doi**: 10.1016/j.ejmech.2015.10.022] [**pmid**: 26496013]
15. Nqoro X, Tobeka N, Aderibigbe BA. Quinoline-Based Hybrid Compounds with Antimalarial Activity. Molecules. 2017;**22**(12): 2268. [**doi**: 10.3390/molecules22122268] [**pmid**: 29257067]
16. Surabhi S, Singh BK. Computer aided drug design: an overview. Journal of Drug delivery and Therapeutics. 2018;**8**(5):504-9. [**doi**: 10.22270/jddt.v8i5.1894]
17. Zhang SJ, Le ZG. A simple and selective procedure for α-bromination of alkanones with [Bmim] Br3 as a promoter under solvent-free conditions. Chin Chem Lett. 2005;**16**(12):1590-2. [Link]
18. Zhao X, Li YF, Zhang SJ, Shao Y, Wang XL. Synthesis and characterization of novel polyimides derived from 2-amino-5-[4-(4′-aminophenoxy) phenyl]-thiazole with some of dianhydride monomers. Polymer. 2007;**48**(18):5241-9. [**doi**: 10.1016/j.polymer.2007.07.001]
19. Xu Q, Huang L, Liu J, Ma L, Chen T, Chen J, Peng F, Cao D, Yang Z, Qiu N, Qiu J, Wang G, Liang X, Peng A, Xiang M, Wei Y, Chen L. Design, synthesis and biological evaluation of thiazole- and indole-based derivatives for the treatment of type II diabetes. Eur J Med Chem. 2012;**52**:70-81. [**doi**: 10.1016/j.ejmech.2012.03.006] [**pmid**: 22483089]
20. Kidwai M, Bhatnagar D, Mothsra P, Singh AK, Dey S. Molecular iodine as a versatile reagent for Hantzsch synthesis of 2-

aminothiazole derivatives. Journal of Sulfur Chemistry. 2009;**30**(1):29-36. [**doi**: 10.1080/17415990802422365]
21. Abdel-Aziz SA, Salem OI, Bakr AG, Sayed IM. Facile synthesis, molecular docking, and biological screening of 1, 3-disubstituted urea derivatives. J Chem Pharm Res. 2014;**6**(10):172-83. [Link]
22. Michael R.B. The NCI In Vitro Anticancer Drug Discovery Screen. Concept, Implementation, and Operation, 1985-1995
23. Kaoud TS, Devkota AK, Harris R, Rana MS, Abramczyk O, Warthaka M, Lee S, Girvin ME, Riggs AF, Dalby KN. Activated ERK2 is a monomer in vitro with or without divalent cations and when complexed to the cytoplasmic scaffold PEA-15. Biochemistry. 2011;**50**(21):4568-78. [**doi**: 10.1021/bi200202y] [**pmid**: 21506533]
24. Madsen JA, Kaoud TS, Dalby KN, Brodbelt JS. 193-nm photodissociation of singly and multiply charged peptide anions for acidic proteome characterization. Proteomics. 2011;**11**(7):1329-34. [**doi**: 10.1002/pmic.201000565] [**pmid**: 21365762]
25. Yan C, Kaoud T, Lee S, Dalby KN, Ren P. Understanding the specificity of a docking interaction between JNK1 and the scaffolding protein JIP1. J Phys Chem B. 2011;**115**(6):1491-502. [**doi**: 10.1021/jp1073522] [**pmid**: 21261310]
26. Kaoud TS, Park H, Mitra S, Yan C, Tseng CC, Shi Y, Jose J, Taliaferro JM, Lee K, Ren P, Hong J, Dalby KN. Manipulating JNK signaling with (--)-zuonin A. ACS Chem Biol. 2012;**7**(11):1873-83. [**doi**: 10.1021/cb300261e] [**pmid**: 22916726]
27. Lee S, Warthaka M, Yan C, Kaoud TS, Ren P, Dalby KN. Examining docking interactions on ERK2 with modular peptide substrates. Biochemistry. 2011;**50**(44):9500-10. [**doi**: 10.1021/bi201103b] [**pmid**: 21955038]
28. Ashry M, Askar H, Alian A, Zidan SA, El-Sahra DG, Abdel-Wahhab KG, Lamlom SF, Abdelsalam NR, Abd El-Hack ME, Gomaa HF. The antioxidant and antitumor efficiency of *Litophyton* sp. extract in DMH-induced colon cancer in male rats. Life. 2022;**12**(10):1470. [**doi**: 10.3390/life12101470]
29. Perandones CE, Illera VA, Peckham D, Stunz LL, Ashman RF. Regulation of apoptosis in vitro in mature murine spleen T cells. J Immunol. 1993;**151**(7):3521-9. [**pmid**: 8376790]
30. Carleton HM, RAB Drury, EA Wallington. Carleton's histological technique. Oxford University Press. USA.1980. [Link]
31. Steel RG, Torrie JH. Principles and procedures of statistics.1960. [Link]
32. Pommier Y. DNA topoisomerases and cancer. Berlin, Germany. Springer. 2012. [Link]
33. Wang JC. Cellular roles of DNA topoisomerases: a molecular perspective. *Nat Rev Mol Cell Biol*. 2002;**3**(6):430-40. [**doi**: 10.1038/nrm831]
34. Barker CR, McNamara AV, Rackstraw SA, Nelson DE, White MR, Watson AJ, Jenkins JR. Inhibition of Hsp90 acts synergistically with topoisomerase II poisons to increase the apoptotic killing of cells due to an increase in topoisomerase II mediated DNA damage. Nucleic Acids Res. 2006;**34**(4):1148-57. [**doi**: 10.1093/nar/gkj516] [**pmid**: 16504968]
35. Lee J, Kim KH, Jeong S. Discovery of a novel class of 2-aminopyrimidines as CDK1 and CDK2 inhibitors. Bioorg Med Chem Lett. 2011;**21**(14):4203-5. [**doi**: 10.1016/j.bmcl.2011.05.081] [**pmid**: 21684737]
36. Payton M, Chung G, Yakowec P, Wong A, Powers D, Xiong L, Zhang N, Leal J, Bush TL, Santora V, Askew B, Tasker A, Radinsky R, Kendall R, Coats S. Discovery and evaluation of dual CDK1 and CDK2 inhibitors. Cancer Res. 2006;**66**(8):4299-308. [**doi**: 10.1158/0008-5472.CAN-05-2507] [**pmid**: 16618755]
37. Zegzouti H, Zdanovskaia M, Hsiao K, Goueli SA. ADP-Glo: A Bioluminescent and homogeneous ADP monitoring assay for kinases. Assay Drug Dev Technol. 2009;**7**(6):560-72. [**doi**: 10.1089/adt.2009.0222] [**pmid**: 20105026]
38. Morgan DO, Fisher RP, Espinoza FH, Farrell A, Nourse J, Chamberlin H, Jin P. Control of eukaryotic cell cycle progression by phosphorylation of cyclin-dependent kinases. Cancer J Sci Am. 1998;**4**:S77-83. [**pmid**: 9619275]
39. Hassan AA, Aly AA, Mohamed NK, El Shaieb KM, Makhlouf MM, Abdelhafez EMN, et.al. Design, synthesis, and DNA interaction studies of furo-imidazo[3.3.3]propellane derivatives: Potential anticancer agents. Bioorg Chem. 2019;**85**:585-99. [**doi**: 10.1016/j.bioorg.2019.02.027] [**pmid**: 30878891]
40. Ruetz S, Fabbro D, Zimmermann J, Meyer T, Gray N. Chemical and biological profile of dual Cdk1 and Cdk2 inhibitors. Curr Med Chem Anticancer Agents. 2003;**3**(1):1-14. [**doi**: 10.2174/1568011033353605] [**pmid**: 12678910]
41. Muthu R, Selvaraj N, Vaiyapuri M. Anti-inflammatory and proapoptotic effects of umbelliferone in colon carcinogenesis. Hum Exp Toxicol. 2016;**35**(10):1041-54. [**doi**: 10.1177/0960327115618245] [**pmid**: 26655637]
42. Kim NH, Lee MY, Park JH, Park DI, Sohn CI, ChoiK, Jung YS. Serum CEA and CA 19-9 Levels are Associated with the Presence and Severity of Colorectal Neoplasia. Yonsei Med J. 2017;**58**: 918-24. [**doi**: 10.3349/ymj.2017.58.5.918] [**pmid**: 28792134]
43. Mostafa1 MA, Ismail MM, Morsy JM, Hassanin HM, Abdelrazek MM. Synthesis, characterization, anticancer, and antioxidant activities of chitosan Schif bases bearing quinolinone or pyranoquinolinone and their silver nanoparticles derivatives. Polym Bull. 2023;**80**(4):4035-59. [**doi**: 10.1007/s00289-022-04238-7]
44. Abd-Elmoneim MA, BakarAA, Awad IM, Moharib SA, Mohamed EM. Anticarcinogenic Effect of Raphanus sativus on 1, 2 Dimethylhydrazine (DMH) Induced Colon Cancer in Rats. Egypt J Hosp. Med. 2013; **51**: 473–86. [**doi**: 10.21608/ejhm.2013.15996]
45. Garba S, Adelaiye A, Mshelia L. Histopathological and biochemical changes in the rats kidney following exposure to a pyrethroid based mosquito coil. J Appl Sci Res. 2007;**3**(12):1788-93. [Link]
46. Abdel-Hamid OM, Nafee AA, Emam MA, Elshimaa MA. The ameliorative effect of Vitamin C in experimentally induced colon cancer in rats. Benha Veter Med J. 2018; **34**(1):329-43. [**doi**: 10.21608/bvmj.2018.54257]
47. Yang J, Xiong LJ, Xu F, Zhao X, Liu B, Cai KL, Wang GB. Estrogen inhibits colon polyp formation by reducing angiogenesis in a carcinogen-induced rat model. Int J Endocrinol. 2013;**2013**: 453898. [**doi**: 10.1155/2013/453898] [**pmid**: 24348555]
48. Rytsyk O, Soroka Y, Shepet I, Vivchar Z, Andriichuk I, Lykhatskyi P, Fira L, Nebesna Z, Kramar S, Lisnychuk N. Experimental evaluation of the effectiveness of resveratrol as an antioxidant in colon cancer prevention. Natural product communications. 2020;**15**(6):1934578X20932742.[**doi**: 10.1177/1934578X20932742]
49. Pollack MH, Van Ameringen M, Simon NM, Worthington JW, Hoge EA, Keshaviah A, Stein MB. A double-blind randomized controlled trial of augmentation and switch strategies for refractory social anxiety disorder. Am J Psychiatry. 2014;**171**(1):44-53. [**doi**: 10.1176/appi.ajp.2013.12101353] [**pmid**: 24399428]